HAL
open science

Dispersion characteristics of the flexural wave assessed using low frequency (50–150 kHz) point-contact transducers: A feasibility study on bone-mimicking phantoms

Koussila Kassou, Youcef Remram, Pascal Laugier, Jean-Gabriel Minonzio

▶ To cite this version:

HAL Id: hal-01971770

https://hal.sorbonne-universite.fr/hal-01971770v1

Submitted on 7 Jan 2019

Dispersion characteristics of the flexural wave assessed using low frequency (50–150 kHz) point-contact transducers: A feasibility study on bone-mimicking phantoms

Koussila Kassou [a,*], Youcef Remram [a], Pascal Laugier [b], Jean-Gabriel Minonzio [b]

[a] *Laboratory of Instrumentation (LINS), USTHB, P.O. BOX 32, 16111 Bab-Ezzouar, Algiers, Algeria*
[b] *Sorbonne Universités, UPMC Univ. Paris 06, CNRS, INSERM, Laboratoire d'Imagerie Biomédicale (LIB), F-75006 Paris, France*

ARTICLE INFO

ABSTRACT

Guided waves-based techniques are currently under development for quantitative cortical bone assessment. However, the signal interpretation is challenging due to multiple mode overlapping. To overcome this limitation, dry point-contact transducers have been used at low frequencies for a selective excitation of the zeroth order anti-symmetric Lamb A0 mode, a mode whose dispersion characteristics can be used to infer the thickness of the waveguide. In this paper, our purpose was to extend the technique by combining a dry point-contact transducers approach to the SVD-enhanced 2-D Fourier transform in order to measure the dispersion characteristics of the flexural mode. The robustness of our approach is assessed on bone-mimicking phantoms covered or not with soft tissue-mimicking layer. Experiments were also performed on a bovine bone. Dispersion characteristics of measured modes were extracted using a SVD-based signal processing technique. The thickness was obtained by fitting a free plate model to experimental data. The results show that, in all studied cases, the estimated thickness values are in good agreement with the actual thickness values. From the results, we speculate that *in vivo* cortical thickness assessment by measuring the flexural wave using point-contact transducers is feasible. However, this assumption has to be confirmed by further *in vivo* studies.

1. Introduction

The NIH Consensus Development Panel on Osteoporosis defines osteoporosis as a skeletal disorder characterized by compromised bone strength predisposing a person to an increased risk of fracture. Bone strength is considered to be primarily due to bone density and quality [1]. Dual-X-ray absorptiometry (DXA) has become the clinical gold standard to measure bone mineral density (BMD) [2]. Quantitative ultrasound (QUS) have been introduced in the late 20th century as a new approach to assess bone quality [3]. QUS offers an alternative to DXA, especially in developing countries where dual-X-ray absorptiometry devices are less accessible to the general population.

Development of QUS technologies have led to two main categories of approaches, namely transverse and axial transmission. Transverse transmission techniques are predominantly used to measure skeletal sites with a dominant trabecular structure, such as the *os calcis* at the heel [4]. Axial transmission (AT) techniques have been developed to specifically assess cortical bone of long bones, such as the radius or the tibia. The general principle of these AT techniques is to generate guided waves in the cortical shell and to measure their speed, using a set of transducers in contact with the skin and aligned along the bone axis [5–8]. The development of these AT techniques answers to the crucial need to assess cortical bone, based on the finding that the majority of non-vertebral fractures after 60 years old occur at predominantly cortical sites [9].

Measurements of the velocity of the first arriving signal (FAS) were first described [10]. The measurement of the FAS is quite straightforward, the method is precise and affordable and several equipments have been developed and assessed *in vivo*. The ability of FAS velocity to predict fracture risk has been evidenced in several clinical studies [11,12,5,6]. However, the absence of a comprehensive model for the FAS does not allow inferring from it characteristics of cortical bone such as thickness or porosity [7]. To overcome this limitation, methods have been introduced that exploit a slower wave, identified as the lowest order Lamb anti-symmetric A0 guided mode (or fundamental flexural guided wave) [8,13] whose dispersion characteristics in a low frequency regime

* Corresponding author.
 E-mail address: kkassou@usthb.dz (K. Kassou).

(between 50 and 150 kHz) are mainly determined by cortical thickness.

Various signal processing techniques, such as group velocity filtering [14], crazy climber algorithm or Radon transform, have been proposed for automatic detection of this mode [15,16] and methods were reported to infer from its dispersion characteristics the cortical thickness [14,17]. Although various *ex vivo* studies have successfully been reported [7,15], these approaches are still limited *in vivo* due to modes overlapping [18], which entails difficulties to extract accurately the A0 mode and to measure its frequency-dependent velocity [6,19]. As an alternative solution to post-acquisition signal processing techniques, selective excitation of a given mode, e.g., the fundamental flexural guided wave is possible using angle beam [20], comb transducers [21] phase-delayed techniques [22,23], and dry point-contact transducers [24]. Such selective excitation techniques make it possible to improve the energy of the mode which it is desired to excite, thus facilitating its detection.

An interesting option for an efficient A0 mode selectivity is that using dry point-contact transducers. For low frequency-thickness product values, and with a transducer generating normal traction on the surface, the A0 mode can be generated preferentially [24]. The main advantages of these dry point-contact transducers include the capacity to provide a high particle displacement at their small ends, to excite and measure guided waves at low frequency and the opportunity to be used without employing coupling gel [25–27]. Dry point-contact transducers have already been tested ex vivo to measure the FAS velocity in bone [28,29]. By comparing guided modes measured by dry point-contact transducers to the modes of a free plate model, Lefebvre et al. were able to evaluate mechanical properties like Young's modulus on *ex vivo* bone specimens [25]. Although this was an interesting study, it did not allow concluding that the waveguide properties could be obtained *in vivo* using point-contact transducers. Dry point-contact transducers have also been tested *in vivo* [30]. A flexural wave, similar to the A0 mode, could be observed, despite the presence of the soft tissues between the contact point of the transducers and the bone surface. However, in this study, the authors have limited their work to measuring the velocity of the flexural wave using a time criterion. The mode dispersion characteristics were not assessed nor the properties of the waveguide.

To follow-up upon these results, we hypothesize that the dispersion characteristics of the flexural wave can be assessed using point-contact transducers and that cortical thickness can be deduced from the measurements, even in presence of soft tissue. In this paper, our purpose was to extend the technique by combining dry point-contact transducers to the SVD-enhanced 2-D Fourier transform [31] in order to measure the dispersion characteristics of the flexural mode. The robustness of our approach was assessed on bone-mimicking phantoms covered or not with soft tissue-mimicking layer. Experiments were also performed on a bovine bone. The paper is organized as follows. The experimental set up, the guided wave measurement principles, the model and the thickness estimation method are presented in Section 2. The results of measurement are described and thickness estimations are presented in Section 3. Section 4 discusses the results.

2. Materials and methods

2.1. Experimental setup

Measurements where achieved with a custom-made experimental setup using two horn dry transducers, one being the transmitter, the other the receiver, and their driving electronics (see
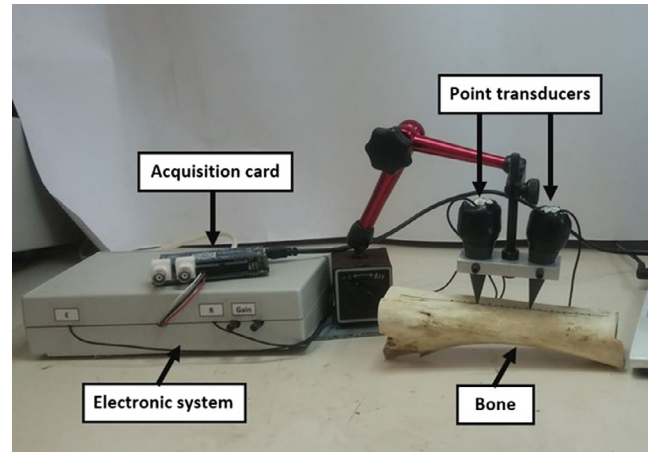

Fig. 1. Experiments measurement fulfilled on bovine bone. Note that the distance between the two transducers varies in these experiments in order to record signals for different spacing between emitter and receiver.

Fig. 1). Signals were recorded using an acquisition card LabTool (Embedded Artists AB, Malmö, Sweden). The system has been developed at the Instrumentation Laboratory (LINS) of the Electronic Department of the Algerian University (USTHB).

The pulser circuit consists of an unstable multivibrator working as a trigger generating step signals (referenced IC3 in Fig. 2(a)). These signals were powered by two transistors (T1 and T2) to produce high-voltage step pulses of 180 V. These pulses are then used to excite the transmitting transducer. The receiver circuit was designed using amplification and filtering stages (Fig. 2(b)). It includes an instrumentation amplifier (AD624, Analog Devices, Norwood, USA) and two amplifiers (TL082, Texas Instruments, Texas, USA) providing variable gain (0–80 dB) and large bandwidth. The low-frequency noise was removed by applying a high-pass filter stage ([C1-R1 and C2-R2] cut-off frequency of 1.5 kHz) before each amplification stage. The power supply of the receiver circuit was insured by two 9-volts batteries. The received signals, before being recorded in data files, were digitized at a 10 MHz-sampling rate using a 12-bits ADC converter of the acquisition card LabTool (Embedded Artists AB, Malmö, Sweden) connected to a laptop via an USB interface. The proposed embedded system is light and compact. It can be powered by 9-volts batteries and boosted to 180 VDC with DC/DC converter and it is therefore a good candidate to be an easily portable bone health assessment device.

The transducers are made of a rectangular shape piezoelectric ceramic ($22 \times 19 \times 8$ mm) bonded to the large section (Fig. 3) of a conical waveguide made of polyvinyl chloride (PVC). The thickness of 8 mm was chosen, adapted to the selected working low frequency regime. The tip of both the transmitter and the receiver are placed on the surface of the specimen, ensuring a contact point with it. The piezoelectric ceramic Pz26 (Ferroperm Piezoceramics A/S, Kvistgaard, Denmark) is protected by silicon and covered with an aluminum sheet for electromagnetic isolation. These transducers allow the measurement in a small localized region (approximately 4 mm^2) without coupling gel and ensure electrical safety for the user and patients. More details about the development steps of these transducers are presented in [32]. Fig. 4 displays the frequency response of the transducer when their tips are in contact and the under 180-Volts unit step excitation. The spectrum contains three vibration modes at low frequency, respectively at 14 kHz, 23 kHz and 33 kHz and a main broadband response ranging from about 70 to 110 kHz. A gap is observed around 50 kHz, associated with a weak sensibility.
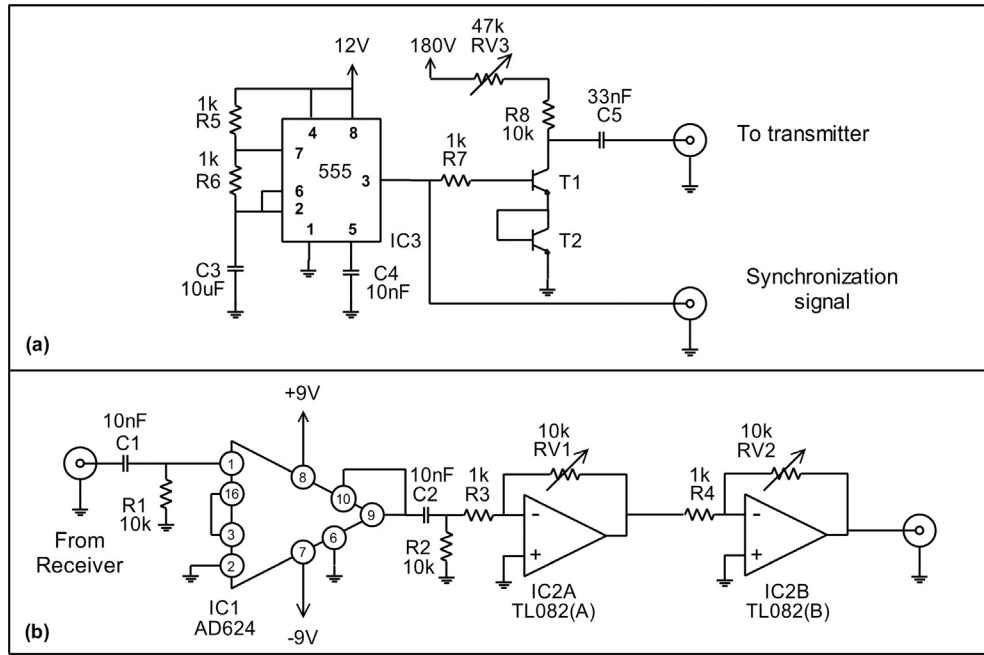
Fig. 2. Electronic schematic of the pulser circuit (a) and of the receiver one (b).
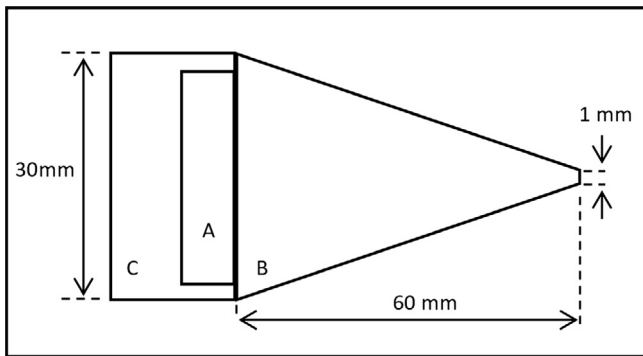
2.2. Bone mimicking-phantoms

The experimental measurements were performed on bone-mimicking plates, and on a bone-mimicking tube. The bone mimicking material (Sawbones (SB), Pacific Research Laboratories Inc., Vashon Island, WA) is composed of short glass fibers embedded in an epoxy matrix. The composite material (mass density $\rho = 1.64$ g.cm^{-3}) is given as transverse isotropic (longitudinal bulk wave velocity parallel to the fibers $V_{L\parallel} = 3570$ m.s^{-1}, longitudinal bulk wave velocity perpendicular to the fibers $V_{L\perp} = 2910$ m.s^{-1}, shear bulk wave velocity $V_T = 1620$ m.s^{-1}) [33,34].

The bone-mimicking plates have been measured first with the transducers tip directly contacting the plate surface. Then, to approach the measuring conditions encountered *in vivo*, the bone mimicking plates were covered with a 5 mm-thick soft tissue-mimicking solid water-based polymer layer (Urethane, CIRS, Norfolk, Virginia, US) (Fig. 5) and the tip of the transducers were placed on the surface of the soft tissue-mimicking layer. At the considered frequencies, the soft tissue-mimicking material

Fig. 3. Point-contact transducer. (A) Rectangular shape piezoelectric ceramic (22 × 19 × 8 mm), (B) conical waveguide and (C) protective cover.
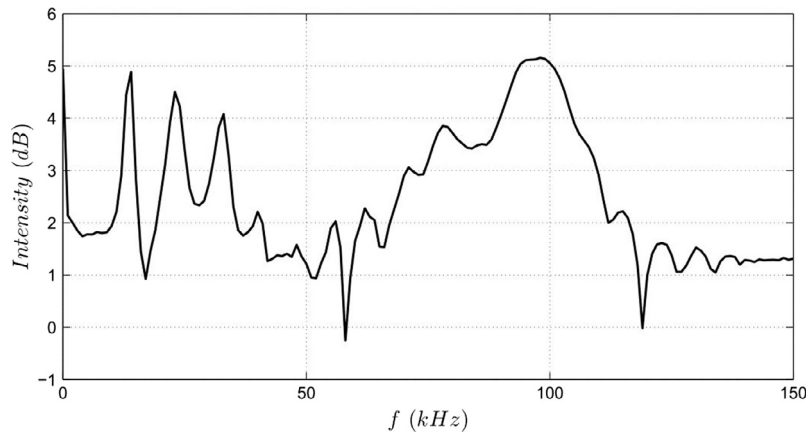

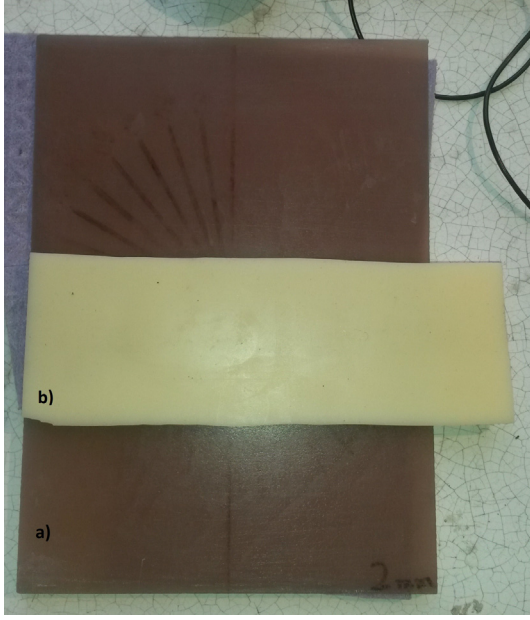**Fig. 4.** Spectral response of conical transducer, when the small ends of transducers were connected together.

Fig. 5. Bone mimicking-plate (Sawbones) of 2.3 mm thick (a) covered with a 5 mm thick soft tissue-mimicking layer (b).

Table 2
Ultrasound-based estimated thickness *usT* (mean ± SD) and reference thicknesses *rT* (mean ± SD) of the bone-mimicking tube and of the bone specimen.

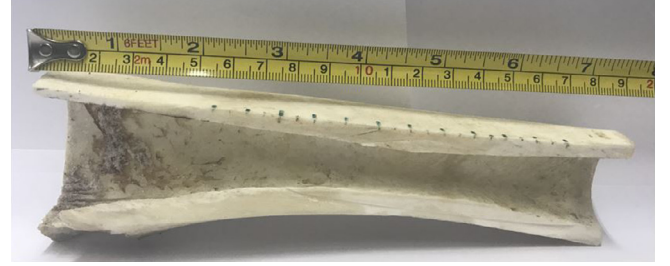|		SB tube	Bone (cortical layer)
Length	L (mm)	500	181
External diameter	D (mm)	35	31–49
Reference thickness	rT (mm)	2.32 ± 0.05	6.29 ± 0.71
Estimated thickness	usT (mm) [by A_0 mode]	2.29 ± 0.085	6.31 ± 0.52

Fig. 6. Bovine bone longitudinally sectioned. Length: 181 mm; outer diameter ranging from 31 to 49 mm; cortical thickness caries between 7.4 mm (middle diaphysis) and 5.0 mm (epiphysis).

behaves acoustically as a fluid [35,36]. The longitudinal velocity $V_{L\ fluid}$ and the attenuation coefficient of Urethane are equal to 1430 m.s^{-1} and 0.9 dB.cm^{-1} at 1 MHz, respectively. Bone mimicking-plate thicknesses were measured ten times at different edges with a precision caliper. Their reference thicknesses (rT) and the mean ($\pm$SD) are given in Table 1. In this work, five bone-mimicking plates with thicknesses ranging from 1 to 10 mm (Table 1) have been measured. The characteristics of the bone-mimicking tube can be found in Table 2.

2.3. Bone preparation

A fresh bovine femur bone was obtained from a local butcher. The soft tissues were carefully removed and the epiphysis are cut off, so that we could concentrate our attention only on cortical bone. After the ultrasonic measurements, the bone has been sectioned longitudinally (Fig. 6) and the reference cortical thickness was measured using a caliper at each ultrasound measurement positions along the bone axis. The reference thickness is given by the mean value of the thickness at the different positions (see Table 2).

2.4. Measurement steps

A straight line was drawn along the fibers direction, i.e., the direction associated with the highest longitudinal bulk velocity, for each bone-mimicking plate and along the axis of the bone-mimicking tube. This line was then graduated every 5 mm. The

ultrasound measurements were performed along these graduations. The transmitter was fixed at a position i and the receiver was displaced along the line with a 5 mm-step. The signal received at positions j was recorded (Fig. 7). The number of transmitter positions N_E was equal to 4. Likewise, the number of receiver positions N_R was equal to 17 for the 10 mm-thick plate and to 19 for all other bone-mimicking samples. The same procedure was applied to the bone specimen with $N_R = 16$. Finally, the temporal matrix response are denoted $r_{ij}(t)$, with i ranging from 1 to N_E, denotes the transmitter index, and j ranging from 1 to N_R, denotes the receiver index.

2.5. Signal processing

Signals $r_{ij}(t)$, with i ranging from 1 to N_E and j ranging from 1 to N_R, denotes temporal matrix response, corresponding to all possible pairs of emitter-receiver positions. In order to extract the experimental dispersion curves, represented by the frequency-dependent wavenumbers, the SVD-based method was applied to $r_{ij}(t)$ matrix following the steps introduced previously [31,34]. These steps are briefly recalled here. First, the matrix response $r_{ij}(t)$ is Fourier transformed in order to obtain the frequency response, noted $R_{ij}(f)$. Secondly, for each frequency, a singular value decomposition (SVD) is applied to the matrix R_{ij}

$$R = \sum_{n=1}^{N_E} U_n \sigma_n^t V_n^* \tag{1}$$

Table 1
Ultrasound-based estimated thickness *usT* (mean ± error of estimate) and reference thicknesses *rT* (mean ± SD) of the bone-mimicking plates.

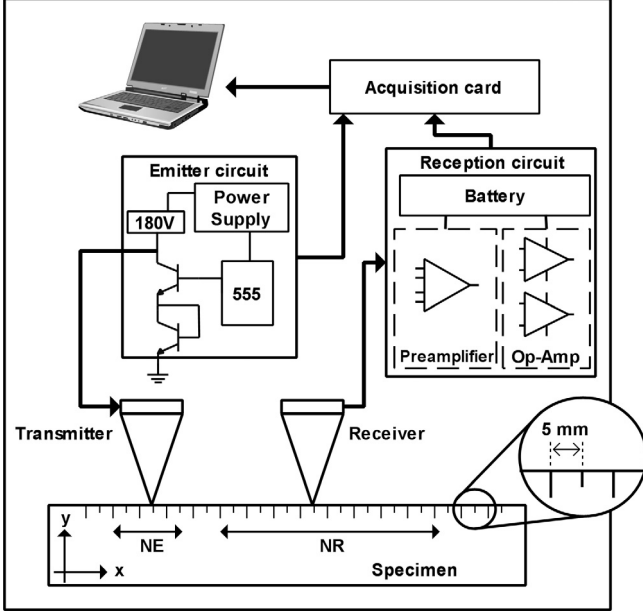|		SB01	SB02	SB03	SB04	SB10
	rT (mm)	1.16 ± 0.05	2.30 ± 0.07	3.29 ± 0.14	4.10 ± 0.04	10.17 ± 0.08
Bone mimicking-plates	usT (mm) [by A_0 mode]	1.15 ± 0.01	2.26 ± 0.05	3.20 ± 0.21	3.90 ± 0.10	7.97 ± 0.53
	usT (mm) [by S_0 mode]	/	/	/	/	9.98 ± 1.57
Bone mimicking-plates covered with fluid layer	usT (mm) [by A_0 mode]	1.14 ± 0.09	2.19 ± 0.09	3.20 ± 0.09	4.17 ± 0.15	10.14 ± 1.31
	usT (mm) [by S_0 mode]	/	/	/	/	9.38 ± 1.30

Fig. 7. Bloc diagram of the system showing the transmitter, the receiver and the measurement principle.

where U_n, V_n and σ_n are respectively the reception singular vectors, the emission singular vectors and the singular values. The notations ^{t} and * denote the transpose and conjugation operations. The reception singular vectors were used to get the so-called Norm function defined by [31].

$$Norm(k,f) = \sum_{n=1}^{M} | \langle U_n | e^{test}(k) \rangle |^2 \qquad (2)$$

The term $\langle U_n | e^{test}(k) \rangle$ denotes the modulus of the Hermitian scalar product between the nth reception singular vector U_n and a testing vector e^{test}, more details on the physical interpretation of the norm function can be found in [31]. If the testing vector is a spatial plane wave of wavenumber k, defined along the N_R receiving positions, then the scalar product is equivalent to the normalized spatial Fourier transform of the reception singular vector U_n. In this study, the testing vector has been modified to take into account the waveguide absorption [37]. The maximum rank M is equal to the number of singular values, *i.e.*, to N_E. A first threshold is applied on the singular values spectrum in order to heuristically determine the rank M at each frequency [31]. Moreover, the *Norm* function values (Eq. (2)) vary from 0 to 1 and reflect the presence rate of the guided waves in the measurements. Thus, a second heuristic threshold is then applied to the Norm function in order to extract the maxima corresponding to the experimental wavenumbers $k_{exp}(f)$. In this work, the second threshold was heuristically fixed equal to 0.4. The discretization steps were chosen equal to $\Delta k = 0.0012$ rad.mm^{-1} and $\Delta f = 250$ Hz.

2.6. Thickness estimation

An inversion scheme was developed in this work to estimate the thickness of the waveguides. For each plate of thickness T, the theoretical guided modes were obtained considering a 2D transverse isotropic non-absorbing free plate model [38]. The inverse fitting mean error $H(T)$ (Eq. (3)) was based on the comparison for each frequency between the theoretical wavenumbers $k_{th}(f)$ and the experimental ones $k_{exp}(f)$.

$$H(T) = \frac{1}{\frac{1}{N_f} \sum_{i=1}^{N_f} | k_{th}(T,f_i) - k_{exp}(f_i) |^2} \qquad (3)$$

where N_f is the number of frequency steps in the bandwidth. It has been observed that $H(T)$ can be approximated by a peak function behavior as illustrated on Fig. 8. The thickness for which the function reaches its maximum is interpreted as the estimated thickness, referred to ultrasonic thickness (*usT*). The half width at half maximum of $H(T)$ defines the estimator resolution and is denoted as the error of estimate in the following.

3. Results

3.1. Bone mimicking-plates

In order to illustrate the effect of the rank M on the *Norm* function Eq. (2), Fig. 9 shows, for the 2.3 mm-thick plate, the *Norm* function reconstructed with two different *M* values [(a) *M* = 4; (b) *M* = 1]. The *Norm* function presents a stronger noise in the *M* = 4 case than in the *M* = 1 case. It is expected as the lower singular values are associated with noise [31]. The noise sources include the electromagnetic disturbances caused by switching power supplies driving the transmitter circuit and the acoustic reverberation caused by plate edges reflections. The noise is illustrated in Fig. 9 (a). Notably, the figure shows the presence of one trajectory with a positive slope corresponding to the dispersive A0 mode and a second line with a negative slope, visible between 0.6 and 1.2 rad.mm^{-1}, corresponding to a mode propagating in the opposite direction, arising from the reflection of the mode A0 at the plate edges. This figure illustrates the ability of the SVD method to separate signal from noise. Almost all the noise was eliminated when only the first singular vector was used, *i.e.*, *M* = 1 Fig. 9(b), compared with the *Norm* function formed with all the singulars vectors, *i.e.*, *M* = 4 Fig. 9(a).

The wavenumbers extracted from the *Norm* function after application of the second threshold, equal to 0.4, are represented in Fig. 10(a) as a function of the frequency. For comparison, the theoretical A0 and S0 guided modes of a 2.3 mm-thick bone-mimicking free plate [38] are also displayed. The experimental wavenumbers $k_{exp}(f)$ are in agreement with the theoretical A0 mode. The experimental mode is discontinuous. The absence of experimental values around 50 kHz is caused by the weak transducers spectral response in the frequency bandwidth as shown in Fig. 4. Only A0 was detected in all plates except for the 10 mm-thick SB plate (Fig. 10(b)), where two trajectories (Tr1 and Tr2), associated with A0 and S0, were detected.

3.2. Bone-mimicking plates covered with a soft-tissue mimicking layer

Fig. 10(c) illustrates the experimental wavenumbers (Tr1, Tr2) of the bilayer waveguide together with the theoretical A0 and S0 modes for the 2.3 mm-thick bone-mimicking plate. Under the hypothesis that the bone mimicking plate and the soft tissue layer can be considered as two independent waveguides [34,35] (*i.e.*, a solid waveguide and a fluid waveguide), the first theoretical (F1) guided mode of a free fluid layer was also calculated and plotted in the same figure for the purpose of comparison. Agreement is obtained between the experimental guided wave (Tr1) and the theoretical A0 mode of the bone mimicking-plate. This result demonstrates the ability of the method to extract the A0 mode from the fluid-SB plate bilayer system. The trajectory Tr2 is identified as the first free fluid mode F1 but deviates from the theoretical curve, likely due to the fluid thickness deformations caused by the point-contact transducers pressure. The trajectory Tr1 only was
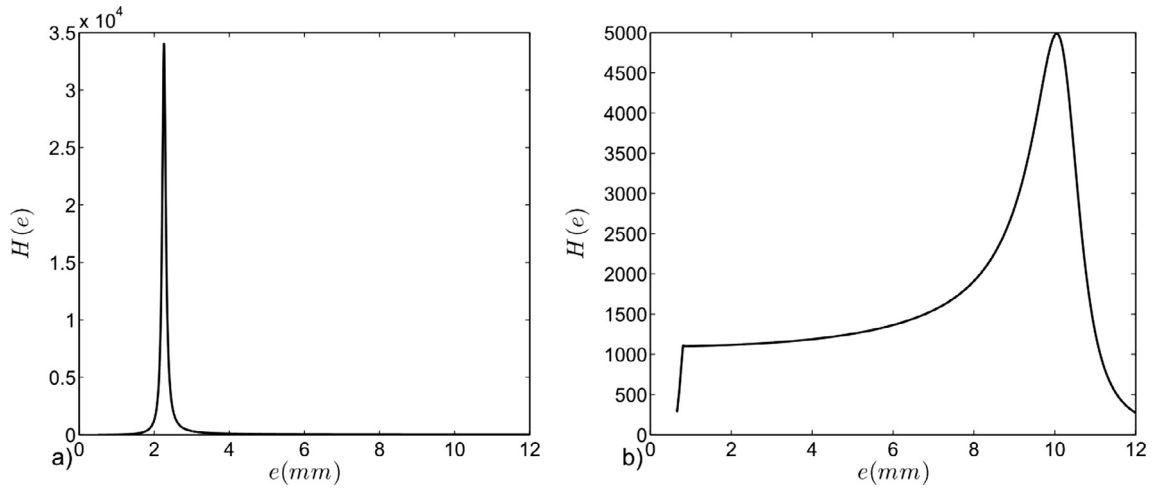
Fig. 8. The inverse fitting mean error $H(T)$ for bone mimicking-plates of thickness equal to 2.3 mm (a) and 10 mm (b).
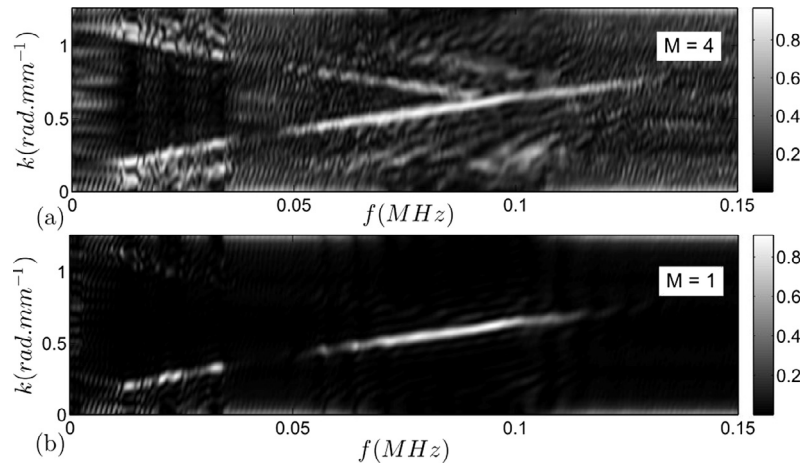

Fig. 9. *Norm*(f,k) functions for a 2.3 mm thick bone mimicking-plate obtained (a) with all singular vectors ($M = 4$) and (b) with only the first singular vector ($M = 1$).
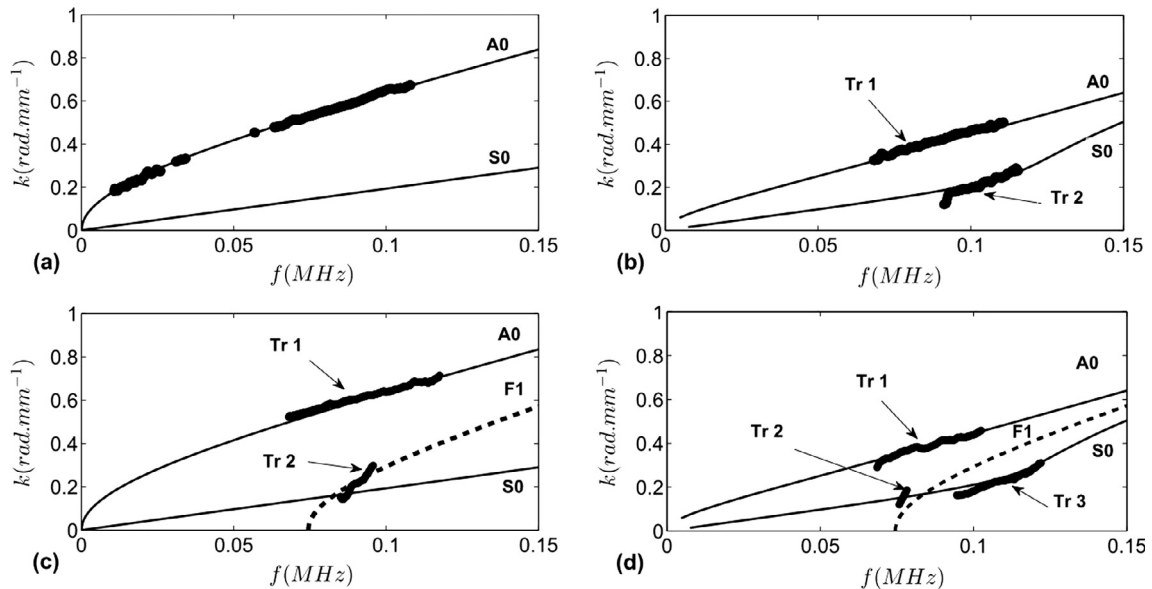

Fig. 10. Experimental wavenumbers (thick dots) compared to the theoretical guided modes of a free plate (thin line) and to the first theoretical mode of a free fluid layer (dashed thick line); (a) and (b) 2.3 mm-thick and 10 mm-thick free plates; (c) and (d) 2.3 mm-thick and 10 mm-thick plates covered with a 5 mm soft tissue-mimicking layer.

used in the inverse scheme to estimate plate thickness. The results are reported in Table 1.

In the case of the 10 mm-thick plate covered by the soft tissue-mimicking layer, the experimental result illustrated on Fig. 10(d) shows the presence of three trajectories. The trajectories Tr1 and Tr3 are clearly associated to A0 and S0. Tr2 corresponds to the first theoretical mode of a free fluid layer. Experimental values are shifted compared to the theoretical ones, probably affected by thickness deformation due to transducers pressure on fluid during the measurements. Both Tr1 and Tr3 were used to estimate the thickness.

3.3. Bone mimicking-tube and bone specimen

The experimental results for the tube and for the bone specimen are presented in Fig. 11(a) and (b), respectively. For the purpose of comparison, the theoretical A0 and S0 modes of a 2.32 mm-thick free plate (corresponding to the thickness of the tube wall) and of a 6.29 mm-thick plate (corresponding to the mean bone cortical thickness), are also represented in Fig. 11(a) and (b), respectively. We notice that, for both results, the experimental guided modes are in agreement with the theoretical modes for frequencies higher than 50 kHz. At low frequency (less than 50 kHz) the experimental trajectories deviate from the theoretical modes. Tr1 and Tr2 were used to estimate the thickness of the tube and the average thickness of cortical bone (Table 2).

3.4. Thicknesses estimation

Table 1 summarizes the estimated values of thickness (usT) and their experimental error compared to the reference thicknesses (rT). For the free bone-mimicking plates, the estimated thickness values are close to the reference thickness values (rT), except for the 10 mm-thick plate. For the particular case of the 10 mm-thick plate, the S0 mode gives a better estimate of the thickness (9.98 mm) than the A0 mode does (7.97 mm).

For the bone mimicking-plates covered with a soft tissue-mimicking layer, including the 10 mm-thick plate, the estimated thickness values are also close to the reference thickness values (rT). In all cases, except for the case of the free 10 mm-thick plate, the thickness of the waveguide was estimated with a relative accuracy error of 1 to 5%. For the bone-mimicking tube and for the bone

specimen, estimated thickness values, presented in Table 2, are close to the reference thickness values.

4. Discussion

For cortical bone characterization, measuring the fundamental flexural mode is particularly interesting at low frequency × thickness product because it is sensitive to the thickness of the cortical waveguide. The thickness can therefore be estimated by using a model, provided that the dispersion characteristics of this particular mode can be accurately measured. Different experimental configurations have been reported to excite and measure the fundamental flexural mode. For example, Moilanen et al., described a technique combining a pair of wideband piezoelectric plane transducers with a varying inter-distance for transmission and reception and a group velocity filtering technique to extract the flexural waveform from the recorded signals and to measure its velocity [6–8,14,15]. However, *in vivo* this approach is limited by the fact that the flexural wave and waves propagating in soft tissue tend to overlap, due to the proximity of their phase velocities and amplitudes. A solution to overcome this limitation is the selective excitation of the flexural wave. Seemingly, this was achieved by using dry point-contact transducers by Tatarinov et al. [30], although there was no clear explanation to the fact that this approach actually favors the flexural mode, diminishing spurious waves propagating in the soft tissues. In this paper, we extend the technique by combining dry point-contact transducers approach to the SVD-enhanced 2-D Fourier transform [31]. The SVD-based method has been used at higher frequencies, *i.e.*, between 0.4 MHz and 2 MHz, to process the signals acquired using a transducer array. This method can be interpreted as an improvement of the classical spatio-temporal Fourier transform [39] adding a denoising step and a mode detection criterion, independent of the mode energy. As opposed to the group velocity filtering technique, our method allows the measurement of guided waves without a priori knowledge on the waveguide or of the velocity of the flexural mode.

For all of the bone mimicking phantoms that we measured, whether they are free or covered with the soft tissue-mimicking layer, a dispersion trajectory was clearly seen in the 2-D Fourier transformed experimental data. The dispersion characteristics of this measured trajectory are in close agreement with those of the theoretical A0 mode. By adjusting the model to the experimental
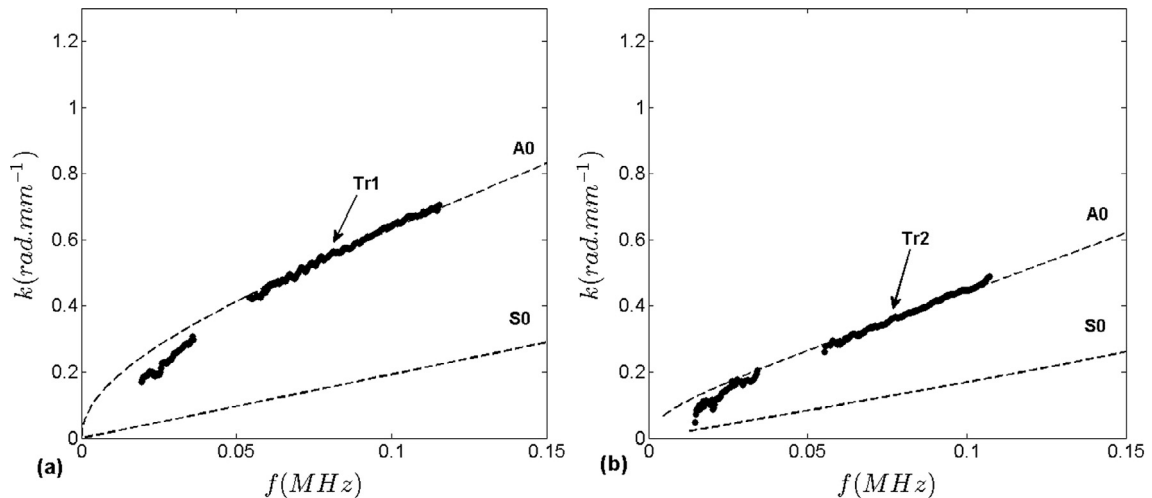

Fig. 11. Experimental wavenumbers (thick dots) for the tube (a) and for the bone specimen (b). Experimental trajectories are compared to the theoretical guided modes (dashed line) of a 2.32 mm-thick bone-mimicking (a) and a 6.29 mm-thick bone (b) free plate, respectively.
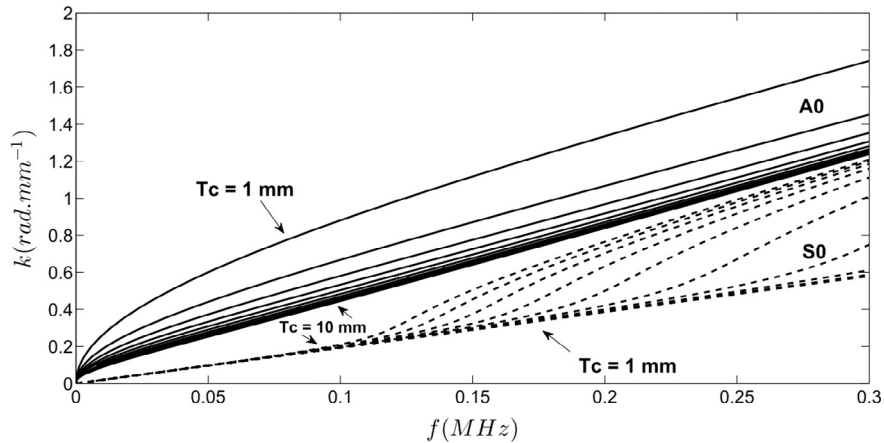
Fig. 12. Dispersion curves for the bone mimicking-plates showing the variation of the dispersion characteristics for A0 (solid line) and S0 (dash line) modes with thickness T ranging from 1 to 10 mm. While the sensitivity to thickness is more pronounced for S0 when the plate thickness gets larger, it is the opposite for A0.

data, the thickness is determined correctly for each case. For thicknesses smaller than 4 mm, accuracy and precision are smaller than 0.2 mm, whereas these values are larger for the 10 mm-thick plate. This can be explained by the fact that the sensitivity to thickness of the A0 mode decreases as thickness increases. In contrast, the sensitivity of the S0 mode increases with the thickness, especially around 0.15 MHz, as shown in Fig. 12. Such sensitivity of S0 explains why, in the case of the 10 mm-thick free plate, a better estimate of thickness is obtained using S0 and A0. Indeed, for the 10 mm-thick plate, both A0 and S0 modes were detected and their dispersion characteristics were consistent with the theoretical predictions. The observation of two modes (A0 and S0) rather than a single one (A0) in the thick plate has already been reported: when the transmitter and the receiver point-contact transducers are on the same side of plate, the sensitivity of S0 (resp. A0) mode detection increases (resp. decreases) as the frequency × thickness product increases [24]. The 10-mm thick plate was investigated for completeness, although the issue is academic rather than of clinical interest, since the usual cortical thickness of human long bones such as the radius and the tibia fall in the range of 1–6 mm.

As for plates, the experimental wave numbers of the tube and of the bone specimen are also consistent with the theoretical plate A0 mode (Fig. 11). Measurement of guided modes on tubes identified with plate modes has also been observed at higher frequencies [38,40]. However, for frequencies lower than 50 kHz, experimental trajectories deviate from the theoretical plate A0 modes and could be identified better by cylindrical guided modes [8]. From the results on bone-mimicking plates covered by soft tissue-mimicking layer, on a tube and on a bovine bone measured *ex vivo*, we speculate that *in vivo* cortical thickness assessment by measuring the flexural wave using point-contact transducers is feasible. However, this assumption has to be confirmed by further *in vivo* studies.

5. Conclusion

In this work, we proposed a low frequency axial transmission device, using point-contact transducers. The device showed its capacity to generate selectively the zero order anti-symmetric Lamb A0 mode in all tested specimens, a mode which can be used to infer, from its dispersion characteristics, the thickness of the waveguide. Measurements of bone mimicking-plates, of bone mimicking-plates covered with a soft tissue-mimicking layer, of bone mimicking-tube and of cortical bone have been achieved. In all cases, the thickness of the waveguide was estimated with a rel-

ative accuracy error of 1–5%. For the thickest plate (10 mm), both A0 and S0 modes were generated. In this last case, because the dispersion of A0 is weak, S0 was used to estimate thickness. Importantly, our study demonstrates that the thickness could be estimated despite the presence of a soft tissue-mimicking layer on top of the plates. For future studies, the design of the system can be improved by adding more point-contact transducers to allow an easy back and forth scanning and a shorter scan time. Furthermore, the frequency bandwidth of the point-contact transducers can be increased to get more experimental values in the selected mode and therefore increasing precision of measurement.

References

[1] NIH Consensus Development Panel on Osteoporosis Prevention, Diagnosis, and Therapy, Osteoporosis prevention, diagnosis, and therapy, JAMA 285 (2001) 785–795.

[2] John A Kanis, Diagnosis of osteoporosis and assessment of fracture risk, Lancet 359 (2002) 1929–1936.

[3] P. Laugier, Quantitative ultrasound instrumentation for bone in vivo characterization, in: P. Laugier, G. Haiat (Eds.), Bone Quantitative Ultrasound, Springer, New York, 2010, p. 48 (Chapter 3).

[4] D. Hans, P. Dargent-Molina, A. Schott, J. Sebert, C. Cormier, P. Kotzki, P. Delmas, J. Pouilles, G. Breart, P. Meunier, heel measurements to predict hip fracture in elderly women: the EPIDOS prospective study, Lancet 348 (1996) 511–514.

[5] M. Talmant, S. Kolta, Ch. Roux, D. Haguenauer, I. Vedel, B. Cassou, E. Bossy, P. Laugier, In vivo performance evaluation of bi-directional ultrasonic axial transmission for cortical bone assessment, Ultrasound Med. Biol. 35 (2009) 912–919.

[6] P. Moilanen, M. Maatta, V. Kilappa, L. Xu, P.H.F. Nicholson, M. Alén, J. Timonen, T. Jamsa, S. Cheng, Discrimination of fractures by low-frequency axial transmission ultrasound in postmenopausal females, Osteoporos Int. 24 (2013) 723–730.

[7] M. Muller, P. Moilanen, E. Bossy, P. Nicholson, V. Kilappa, J. Timonen, M. Talmant, S. Cheng, P. Laugier, Comparison of three ultrasonic axial transmission methods for bone assessment, Ultrasound Med. Biol. 31 (2005) 633–642.

[8] P.H.F. Nicholson, P. Moilanen, T. Karkkainen, J. Timonen, S. Cheng, Guided ultrasonic waves in long bones: modelling, experiment and in vivo application, Physiol. Meas. 23 (2002) 755–768.

[9] R.M.D. Zebaze, A. Ghasem-Zadeh, A. Bohte, S. Iuliano-Burns, M. Mirams, R.I. Price, E.J. Mackie, E. Seeman, Intracortical remodelling and porosity in the distal radius and post-mortem femurs of women: a cross-sectional study, Lancet 375 (2010) 1729–1736.

[10] A.J. Foldes, A. Rimon, D.D. Keinan, M.M. Popovtzer, Quantitative ultrasound of the tibia: a novel approach for assessment of bone status, Bone 17 (1995) 363–367.

[11] D. Hans, S.K. Srivastav, C. Singal, R. Barkmann, C.F. Njeh, E. Kantorovich, C. C Glüer, H. K Genant, Does combining the results from multiple bone sites measured by a new quantitative ultrasound device improve discrimination of hip fracture?, J Bone Miner Res. 14 (1999) 644–651.

[12] R. Barkmann, E. Kantorovich, C. Singal, D. Hans, H.K. Genant, M. Heller, C.C. Glüer, A new method for quantitative ultrasound measurements at multiple skeletal sites: first results of precision and fracture discrimination, J. Clin. Densitom. 3 (2000) 1–7.

[13] M. Sasso, M. Talmant, G. Haiat, S. Naili, P. Laugier, Analysis of the most energetic late arrival in axially transmitted signals in cortical bone, IEEE Trans. Ultrason. Ferroelectr. Freq. Control. 56 (2009) 2463–2470.

[14] P. Moilanen, P.H. Nicholson, V. Kilappa, S. Cheng, J. Timonen, Measuring guided waves in long bones: modeling and experiments in free and immersed plates, Ultrasound Med. Biol. 5 (2006) 709–719.

[15] V. Kilappa, K. Xu, P. Moilanen, E. Heikkola, D. Ta, J. Timonen, Assessment of the fundamental flexural guided wave in cortical bone by an ultrasonic axial-transmission array transducer, Ultrasound Med. Biol. 36 (2013) 1223–1232.

[16] K. Xu, D. Ta, D. Cassereau, B. Hu, W. Wang, P. Laugier, J.G. Minonzio, Multichannel processing for dispersion curves extraction of ultrasonic axial-transmission signals: comparisons and case studies, J. Acoust. Soc. Am. 140 (2016) 1758–1770.

[17] P. Moilanen, M. Talmant, P.H.F. Nicholson, S. Cheng, J. Timonen, P. Laugier, Ultrasonically determined thickness of long cortical bones: three-dimensional simulations of in vitro experiments, J. Acoust. Soc. Am. 122 (2007) 2439–2445.

[18] P. Moilanen, M. Talmant, V. Kilappa, P. Nicholson, S. Cheng, J. Timonen, P. Laugier, Modeling the impact of soft tissue on axial transmission measurements of ultrasonic guided waves in human radius, J. Acoust. Soc. Am. 124 (2008) 2364–2373.

[19] V. Kilappa, P. Moilanen, L. Xu, P.H.F. Nicholson, J. Timonen, S. Cheng, Low-frequency axial ultrasound velocity correlates with bone mineral density and cortical thickness in the radius and tibia in pre- and postmenopausal women, Osteoporos Int. 22 (2011) 1103–1113.

[20] D. Ta, W. Wang, Y. Wang, L.H. Le, Y. Zhou, Measurement of the dispersion and attenuation of cylindrical ultrasonic guided waves in long bone, Ultrasound Med. Biol. 35 (2009) 641–652.

[21] J.L. Rose, S.P. Pelts, J.N. Barshinger, M.J. Quarry, An ultrasonic comb transducer for guided wave mode selection in materials characterization, in: Robert E. Green (Ed.), Nondestructive Characterization of Materials VIII, Springer, US, 1998, p. 697, Chapter: Materials Characterization I.

[22] P. Moilanen, Z. Zhao, P. Karppinen, T. Karppinen, V. Kilappa, J. Pirhonen, R. Myllyla, E. Haeggstrom, J. Timonen, Photo-acoustic excitation and optical detection of fundamental flexural guided wave in coated bone phantoms, Ultrasound Med. Biol. 40 (2014) 521–531.

[23] P. Karppinen, A. Salmi, P. Moilanen, T. Karppinen, Z. Zhao, R. Myllyla, J. Timonen, E. Haeggstrom, Phase-delayed laser diode array allows ultrasonic guided wave mode selection and tuning, J. Appl. Phys. 113 (2013) 144904.

[24] F. Levent Degertekin, Butrus T. Khuri-Yakub, Single mode Lamb wave excitation in thin plates by Hertzian contacts, Appl. Phys. Lett. 69 (1996) 146–148.

[25] F. Lefebvre, Y. Deblock, P. Campistron, D. Ahite, J.J. Fabre, Development of a new ultrasonic technique for bone and biomaterials in vitro characterization, J. Biomed. Mater. Res. 63 (2002) 441–446.

[26] Z. Fu, X. Xian, S. Lin, C. Wang, W. Hu, G. Li, Investigations of the barbell ultrasonic transducer operated in the full-wave vibrational mode, Ultrasonics 52 (2012) 578–586.

[27] D. Ensminger, Solid cone in longitudinal half-wave resonance, J. Acoust. Soc. Am. 32 (1960) 194–196.

[28] H. Jansons, A. Tatarinov, V. Dzenis, A. Kregers, Constructional peculiarities of the ham tibia dewed by reference to ultrasound measurement data, Biomaterials 5 (1984) 221–226.

[29] Y. Remram, M. Attari, N. Ababou, Determination of relationships between the ultrasound velocity and the physical properties of bovine cortical bone femur, Iran. Biomed. J. 11 (2007) 193–198.

[30] A. Tatarinov, A. Sarvazyan, Topography of acoustical properties of long bones: from biomechanical studies to bone health assessment, IEEE Trans. Ultrason. Ferroelectr. Freq. Control. 55 (2008) 1287–1297.

[31] J.-G. Minonzio, M. Talmant, P. Laugier, Guided wave phase velocity measurement using multi-emitter and multi-receiver arrays in the axial transmission conguration, J. Acoust. Soc. Am. 127 (2010) 2913–2919.

[32] K. Koussila, Y. Remram, Development of electronic system for velocity ultrasound measurement: in vitro bone studies, in: 8th International Conference on Modelling, Identification and Control (ICMIC), Algiers, 2016, pp. 406–411.

[33] S. Bernard, Q. Grimal, P. Laugier, Resonant ultrasound spectroscopy for viscoelastic characterization of anisotropic attenuative solid materials, J. Acoust. Soc. Am. 135 (2014) 2601–2613.

[34] N. Bochud, Q. Vallet, J.-G. Minonzio, P. Laugier, Genetic algorithms-based inversion of multimode guided waves for cortical bone characterization, Phys. Med. Biol. 61 (2016) 6953–6974.

[35] J. (Chen), J. Foiret, J.-G. Minonzio, M. Talmant, Z. Su, L. Cheng, P. Laugier, Measurement of guided mode wavenumbers in soft tissue-bone mimicking phantoms using ultrasonic axial transmission, Phys. Med. Biol. 57 (2012) 3025–3037.

[36] N. Bochud, Q. Vallet, J.-G. Minonzio, P. Laugier, Predicting bone strength with ultrasonic guided waves, Scientific Rep. 7 (2017) 43628.

[37] J.-G. Minonzio, J. Foiret, M. Talmant, P. Laugier, Impact of attenuation on guided mode wavenumber measurement in axial transmission on bone mimicking plates, J. Acoust. Soc. Am. 130 (2011) 3574–3582.

[38] J. Foiret, J.-G. Minonzio, C. Chappard, M. Talmant, P. Laugier, Combined estimation of thickness and velocities using ultrasound guided waves: a pioneering study on in vitro cortical bone samples, IEEE Trans. Ultrason. Ferroelectr. Freq. Control. 61 (2014) 1478–1488.

[39] D. Alleyne, P. Cawley, A two-dimensional Fourier transform method for the measurement of propagating multimode signals, J. Acoust. Soc. Am. 89 (1991) 1159.

[40] J.-G. Minonzio, J. Foiret, P. Moilanen, J. Pirhonen, Z. Zhao, M. Talmant, J. Timonen, P. Laugier, A free plate model can predict guided modes propagating in tubular bone-mimicking phantoms, J. Acoust. Soc. Am. 137 (2015) EL98–EL104.